Physics of Plasmas ARTICLE scitation.org/journal/php

# Positron orbit effects during injection and confinement in a magnetic dipole trap

Cite as: Phys. Plasmas **27**, 052107 (2020); doi: 10.1063/5.0007252
Submitted: 10 March 2020 · Accepted: 23 April 2020 ·
Published Online: 19 May 2020



S. Nißl,[1,2,a] E. V. Stenson,[1,2,3,b] U. Hergenhahn,[1,c] J. Horn-Stanja,[1] T. Sunn Pedersen,[1,4] H. Saitoh,[5] C. Hugenschmidt,[2] M. Singer,[2] M. R. Stoneking,[1,6] and J. R. Danielson[3]

## AFFILIATIONS

[1]Max Planck Institute for Plasma Physics, 17491 Greifswald, Germany and 85748 Garching, Germany
[2]Technische Universität München, 85748 Garching, Germany
[3]University of California San Diego, La Jolla, California 92093, USA
[4]University of Greifswald, 17489 Greifswald, Germany
[5]The University of Tokyo, 277-8561 Kashiwa, Japan
[6]Lawrence University, Appleton, Wisconsin 54911, USA

**Note:** This paper is part of the Special Collection: Papers from the 61st Annual Meeting of the APS Division of Plasma Physics.
**Note:** Paper BI3 3, Bull. Am. Phys. Soc. **64** (2019).
[a]**Author to whom correspondence should be addressed:** stefan.nissl@ipp.mpg.de
[b]Invited speaker.
[c]**Also at:** Fritz-Haber-Institut der Max-Planck-Gesellschaft, 14195 Berlin, Germany.

## ABSTRACT

Lossless injection of positrons into a magnetic dipole trap and their subsequent confinement have been demonstrated. Here, we investigate by numerical single-particle simulations how the radial distribution of positrons in the trap is affected by the measurement itself, the choice of injection parameters, the asymmetry of the electric potential, and by elastic collisions. The results are compared to experimental data. A comprehensive understanding of these effects is a milestone on the road to creating an electron–positron plasma in a trap with a levitating superconducting coil.



## I. INTRODUCTION

In contrast to an electron–ion plasma, a "pair plasma" consists of particle species with opposite charge but with the same mass. Because of this mass equality, it is predicted that pair plasmas exhibit novel behavior, including simpler dispersion relations[1] and extraordinary stability properties in certain regimes.[2] Despite being a test bed for general plasma physics as well as astrophysics, pair plasmas have been studied[3,4] relatively little in laboratories to date, due to the significant experimental challenges involved, especially the scarcity of antimatter.

The goal of A Positron–Electron eXperiment (APEX)[5] is the creation of a magnetized, low-energy pair plasma by confining electrons and positrons in a dipole magnetic field produced by a levitating superconducting coil.[6–9] The dipole was chosen due to its capability to confine plasmas with an arbitrary degree of non-neutrality.[10,11] Another configuration with this property is the stellarator, which is also being developed in conjunction with the dipole.[12] In the test setup Proto-APEX that uses a supported permanent magnet, we have already demonstrated efficient injection of a positron beam[13] and confirmed that injected positrons can be confined for more than a second.[14] In parallel, efficient particle trajectory simulations have been developed that reproduce and thereby explain experimental findings.

This paper expands upon and extends these previous results. First, we argue that the probe, used to measure the radial distribution of positrons in the trap, works well, despite perturbing the electric potential. We discuss how the radial distribution of injected positrons is affected by certain free parameters of the experiment, as well as how the radial distribution evolves during the drift around the magnet and how it is changed by elastic collisions with residual neutral gas. Furthermore, the effective potential energy is found to be a useful tool to describe the motion of a charged particle in a static electromagnetic

field. Finally, a summary of the conclusions from the current study will be presented.

## II. EXPERIMENTAL SETUP

At the center of Proto-APEX (Fig. 1) is a neodymium permanent magnet (height: 40 mm and diameter: 28 mm), enclosed in a copper case, that provides the dipole magnetic field with a strength of 600 mT at its poles. It is surrounded by a cylindrical wall (radius: 9 cm) divided into multiple electrodes. The lower part consists of eight identical segments while the upper part is split into a 1/8th and 7/8th segment, with the smaller one (labeled Top1) located closest to the injection region. Positrons produced by the NEutron induced POsitron Source MUniCh (NEPOMUC)[15] are guided magnetically to the experiment. NEPOMUC can deliver up to $1 \times 10^9 e^+/s$ with a kinetic energy of 1000 eV (the "primary beam," which has recently been used also at lower energies[16]). Alternatively, the "remoderated beam" is available down to 5 eV at an intensity up to $4 \times 10^7 e^+/s$ after an additional moderation step;[17] this was used for the work described here, due to its smaller diameter and energy spread. The beam enters the experimental setup from above. First, it encounters a diagnostic region containing a movable target plate with an attached micro-channel plate detector (MCP); the beam position and shape can be imaged with the MCP and the positron flux can be determined by measuring the current to and the annihilation gamma ray signal from the target plate. With the diagnostics retracted, the positron beam passes a pair of steering coils that are used to adjust the injection position in radial (r) and azimuthal ($\theta$) directions relative to the symmetry axis of the magnet.

As the positrons enter the main chamber, a pair of oppositely biased electrodes provide the necessary electric field for the positrons to $E \times B$ drift onto field lines that intersect only the magnet. Biasing certain outer wall electrodes [especially, the upper (Top1) and lower (RW1) segments next to the injection region] dramatically improves the injection efficiency.[13] A grounded shield plate helps to reduce the extent to which the strong electric field of the $E \times B$ plates perturbs particle orbits outside the injection region. After injection, positrons execute bounce motion between the polar regions of the magnet while drifting toroidally around it due to the curvature and gradient drift. A target probe can be inserted opposite to the injection region to intercept their flight. With this probe, the integrated radial profile of the positrons can be determined by measuring the current reaching the probe or counting the annihilations seen by a bismuth germanate (BGO) detector whose view is collimated on the probe.

When electrodes are biased statically, injected positrons are lost after they drift around the magnet and experience the electric field of the injection region again (more about this is given in Sec. VI). To study longer confinement times, a so-called "fill-hold-dump" scheme[14] was employed. The positron beam was injected and after some time, the beam was blocked while all electrodes, except the magnet, were grounded. This traps a few hundred positrons in an almost symmetric electromagnetic field. After a variable hold time, the electrodes are switched on again, which forces the confined positrons to be lost. Repeating this cycle a few thousand times for each set of different hold times results in a measurement of how the positron content decays over time.

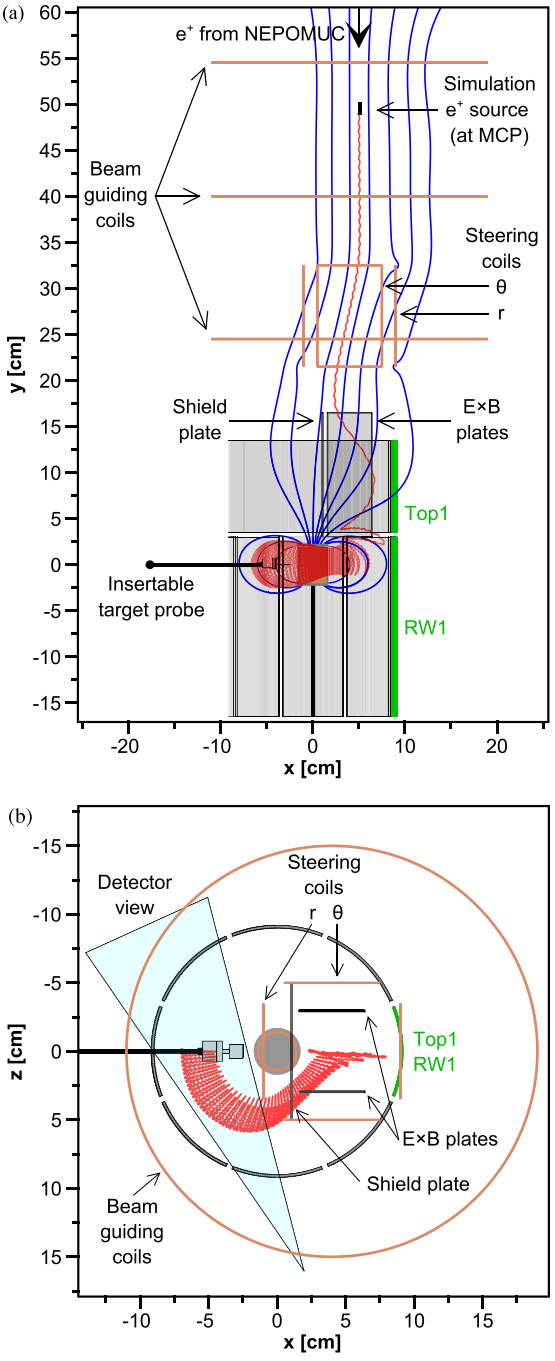


**FIG. 1.** Side view (a) and top view (b) of the experiment, as modeled in the simulation program (with the exception of the magnet support rod). Magnetic field lines are depicted in blue and a sample positron trajectory is shown in red.

## III. SIMULATION SETUP

Since both the available positron beam time and the diagnostic capabilities of the experiment are limited, simulations are a very valuable tool to explain the experimental data, answer questions that are

not diagnostically accessible, and design future experiments. Especially, the asymmetry of the trap makes an analytical approach difficult, but due to the low densities, single-particle trajectory simulations are very well-suited for this task.

The setup of the simulation includes the geometry of the trap, the electric and magnetic fields, an efficient and accurate algorithm to propagate particles, and accurate initial beam parameters. Some parameters are idealized in the simulation because they are not known experimentally to high accuracy or may vary from one experimental campaign to the next. These include for example the exact position of the steering coils, a tilt of the permanent magnet, and the position of the MCP relative to the beam line. Not included in the simulations are the support rods of the permanent magnet and the Earth's magnetic field. Furthermore, a more convenient operating principle of the detector is implemented. While the collimated detector in the experiment only registers a small fraction of all annihilation photons (which is compensated by the high positron flux), the detector in the simulation registers every positron from a much smaller number of launched particles that stops inside its field of view.

### A. Magnetic field

In the simulation, three different types of ideal coils are used (Fig. 1) to model the magnetic field of the experiment in a good approximation. Circular coils[18] are used for the end of the beam line that guides the positrons to the main chamber. Four rectangular coils[19] in two pairs represent the steering coils with which the beam position can be adjusted. Finally, the predominant dipole field of the central permanent magnet is approximated by a continuous finite solenoid.[20] The magnetic field is computed analytically at every point of the particle's trajectory. This is feasible by using the arithmetic-geometric mean to efficiently calculate the elliptic integrals appearing in the coil equations.[21]

### B. Electric potential

Since there is no straightforward analytical formula to determine the electric potential at every point in space, it has to be computed iteratively on a grid and estimated between the grid points by trilinear interpolation. Here, a regular cartesian grid with a grid spacing of 1 mm was used, resulting in $(\mathrm{nx}, \mathrm{ny}, \mathrm{nz}) = (201, 401, 201)$ grid points for every variable potential. To include perturbations caused by the target probe, all potentials were recalculated for every new target probe position. A successive over-relaxation scheme[22] was used to solve the Laplace equation. Space charge effects were omitted since all simulations (and experiments to date) are in the single-particle regime.

### C. Particle pusher

To propagate a particle in the electromagnetic field, a variant of the Boris algorithm was chosen.[23] Assuming the force on the particle is dominated by the Lorentz force, the acceleration can be written as $\vec{a} = \frac{d\vec{v}}{dt} = \frac{q}{m}(\vec{E} + \vec{v} \times \vec{B}) = \vec{\Sigma} + \vec{v} \times \vec{\Omega}$. With $\vec{A} = \vec{\Omega}\Delta t/2$ and $\vec{C} = \vec{v}_{old} + \Delta t(\vec{\Sigma} + \vec{v}_{old} \times \vec{\Omega}/2)$, the position and velocity of the next step are given by

$$\vec{v}_{new} = \frac{\vec{C} + \vec{A}(\vec{A} \cdot \vec{C}) - \vec{A} \times \vec{C}}{1 + A^2}, \tag{1}$$

$$\vec{x}_{new} = \vec{x}_{old} + \Delta t \cdot \vec{v}_{new}. \tag{2}$$

The time step $\Delta t$ for the simulations was between $5 \times 10^{-10}$ s and $5 \times 10^{-11}$ s. This is about two orders of magnitude larger than the time step needed for accurate trajectory calculations with the fourth-order Runge–Kutta algorithm. Additionally, the non-relativistic Boris algorithm conserves phase space volume, in contrast to Runge–Kutta.

The confinement simulations also include a simple elastic collision model. In this model, the direction of the velocity vector is periodically randomized while the magnitude is fixed. To speed up the computation time, the collision rate is typically much higher in the simulation than in the experiment. Good agreement between the two is nevertheless found with respect to the number of collisions for which positrons are confined since they operate in the same collisional regime as long as the collision frequency in the simulation is lower than the bounce frequency of the positrons.

### D. Initial starting position and energy distribution

The particle source in the simulations is placed at the y-value of the MCP. The x–z starting position of the simulated positrons is randomly drawn from a spatial distribution that is extracted from a saved MCP image of the beam. It has to be noted that the center of the MCP is not necessarily aligned with the center of the beam line. To determine a potential offset in the x and z coordinates, the position parameters were scanned and the resultant injection efficiencies were compared to the measured experimental values. The offset that best matched the experiment was then fixed for all subsequent simulations.

The initial positron energy distributions in the simulations are based on measurements with a retarding field analyzer.[17] The parallel energy is described by a Gaussian distribution with a mean energy of 5.16 eV and a standard deviation of 0.78 eV, while the perpendicular energy is described by a Boltzmann distribution with a mean energy of 0.78 eV.

## IV. PERTURBATION CAUSED BY THE TARGET PROBE

The insertable target probe allows us to measure the overall injection efficiency, as well as the radial distribution of injected positrons on the opposite side of the trap from where they are injected—i.e., after a 180° toroidal drift. This can be done by either measuring the positron current collected by the probe or by counting the positron annihilation photons with a collimated scintillation detector. A key question that needed to be addressed about this diagnostic was how strongly the positron orbits are perturbed by the insertion of a grounded electrode into the confinement region, which already has a complex 3D electrostatic landscape. Figure 2 shows the simulation results of two extreme cases; one with the magnet biased to 0 V (a) and the other biased to 30 V (b). For each case, three different simulation methods are compared. The data labeled "In" uses the potential calculated with the target probe fully inserted (Fig. 3). The data labeled "Out" does not include the perturbation to the potential produced by the probe (as if it is fully retracted). For the data labeled "Simulation," the potential was recalculated for each indicated probe position and therefore most closely simulates the actual experimental conditions. In the 0 V case [Fig. 2(a)], the three sets of data lie on top of each other. This is not surprising, since the electric potential in this region of the trap is dominated by the potential of the magnet. For the same reason, the radial shift between the simulated cumulative distribution with the target

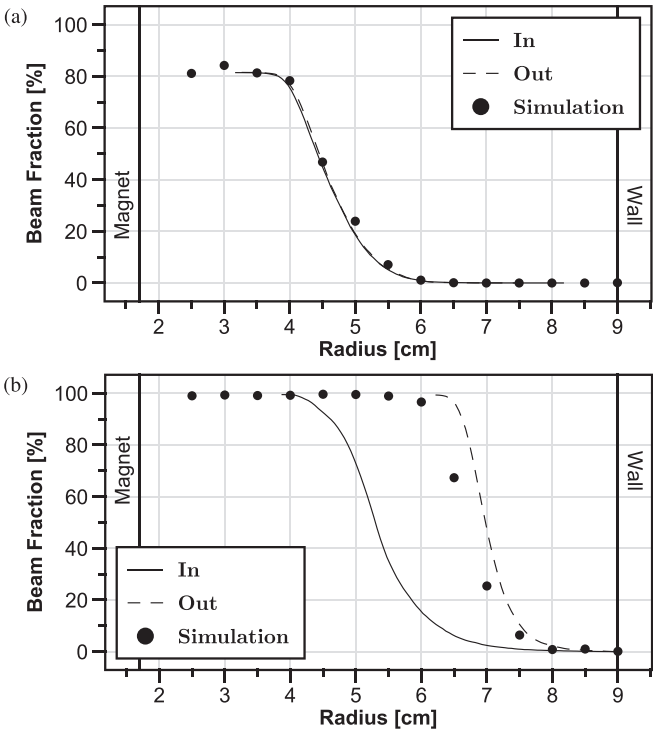


**FIG. 2.** Simulation of the radial positron distribution at a magnetic bias of 0 V (a) and 30 V (b). The dashed line (Out) shows the cumulative distribution in the unperturbed case with the target probe outside. The solid line (In) shows the cumulative distribution of the maximal perturbed case with the target probe fully inserted. The black dots (Simulation) show the simulated counts on a target probe that is inserted stepwise from the wall toward the magnet, like in the experiment. Inserting the probe into the trap creates integrated profiles, so the true radial distributions are their derivatives.

probe outside and fully inserted is significant when the magnet is strongly biased [Fig. 2(b)]. However, since the target probe measurement is performed by inserting it stepwise, the influence on the measurement is considerably smaller ["Simulation" in Fig. 2(b)]. In addition, the radial distribution of injected positrons is localized further from the magnet the higher the magnet bias is—as we will show in Sec. V—which further reduces the perturbation effect. Negative magnet biases have the opposite effect; though a negative bias is beneficial neither for injection nor confinement, it will not be discussed further here.

In Fig. 4, an experimentally measured profile is compared to the simulation. The injection efficiency and the mean location were reproduced by the simulation, albeit the spread of the profile is larger in the experiment than in the simulation. This can be explained by the sensitive initial conditions and by uncertainties of the experiment that are not included in the simulation. For example, a small tilt of the magnet, within the experiment's uncertainty, has been seen to shift and broaden the radial profile.

All this confirms that the target probe, as implemented in our experiment, is a suitable instrument for diagnosing the radial distribution and injection efficiency of positrons, despite the electrostatic potential disturbances it can cause.

## V. MANIPULATION OF THE RADIAL DISTRIBUTION

We have verified in Sec. IV that the radial distribution of positrons in the trap can be measured with the insertable target probe. Knowing the distribution and how to control it is a key factor to design experiments to study the behavior of positrons in the dipole magnetic field. These include, among others, confinement lifetime measurements, in which the radial distribution of trapped positrons affects how long they are confined.[14] For compression experiments that seek to use oscillating wall biases to move particles deeper into the trap, initial profiles centered at larger radii are preferable. For future positron pulse stacking experiments, it might be useful to deposit pulses onto different radii. The main control parameters of the experiment are the steering coil currents $I_r$ and $I_\theta$, the bias voltages of the magnet and the E × B plates, and the biases of the wall segments RW1 and Top1.

To gain insight into the correlation between a free parameter of the system and the resulting radial positron distribution, experiments were conducted by scanning one parameter at a time while inserting the target probe stepwise into the trap, thereby creating a 2D histogram. Consequently, the following measurements show the integrated

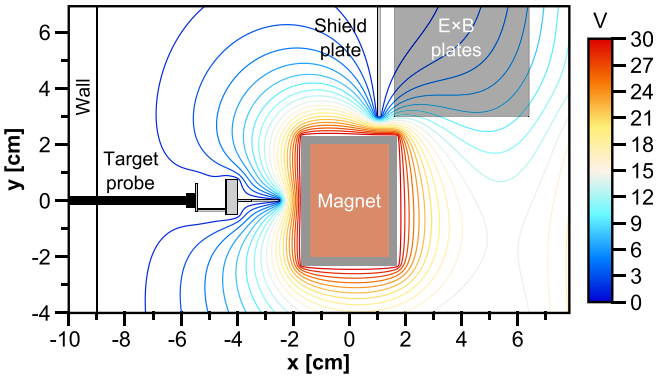


**FIG. 3.** Perturbation of the electric potential caused by the target probe at a magnet bias of 30 V.

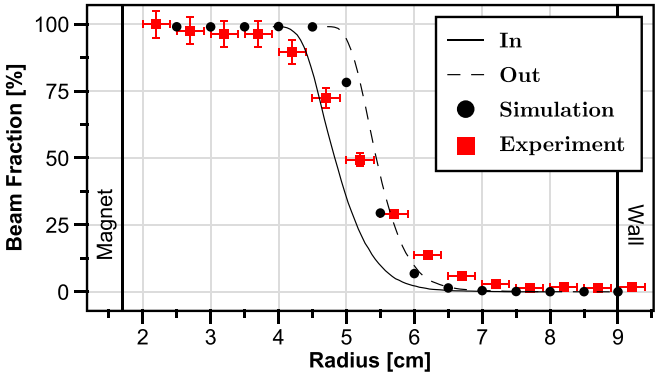


**FIG. 4.** Comparison of an experimentally measured profile (red squares) with the corresponding simulations (black dots). "In" and "Out" are the simulated cumulative distributions with a fully inserted and retracted target probe, respectively. The magnetic bias was 8 V.

distributions, just like the plots in Sec. IV. For the simulations, 200 particles were simulated per bin in the initial parameter space, and the perturbation of the electric field by the target probe was included. The results are shown in Figs. 5–9 and the corresponding parameter settings are listed in Table I (shown in the Appendix).

Figures 5–8 display the comparisons between experiments (a) and simulations (b) for the integrated radial profiles of annihilation counts vs the following control parameters: bias on E × B plates (Fig. 5), bias on the small segment of the top electrode Top1 (Fig. 6), bias on the outer wall segment RW1 (Fig. 7), and bias on the magnet (Fig. 8). Figure 9 shows only simulations for variation in the steering coil currents $I_r$ [Fig. 9(a)] and $I_\theta$ [Fig. 9(b)]. The color scale in all of these figures indicates the fraction of the injected positron beam detected at the target probe. The injection efficiency is determined by the maximum measured/simulated count rate for a given parameter value. For all of these parameter scans, the simulations reproduce the experimental results quite reliably.

Looking at the results in more detail, in the case of 5-eV positrons, an E × B plate voltage between 200 V and 300 V is optimal in terms of injection efficiency. Outside this range, the efficiency drops and the radial positron distribution is more spread out. The signal in the upper right corner is caused by positrons being lost on the wall while still being inside the field of view of the gamma detector. The bias on Top1 does not influence the radial distribution of positrons as long as it is more positive than the beam energy of 5 eV. Changing the bias of the RW1 electrode or the steering coil current $I_\theta$ can shift the profile but only at the cost of a reduced injection efficiency. Changing the bias of the magnet case or the steering coil current $I_r$, however, does shift the radial profile in the range of 1 cm to 2 cm while maintaining a high injection efficiency over a significant range of parameters. The drop of the count rate at high E × B biases/$I_r$ currents and small radii is caused by positrons with a distance between midplane crossings large enough to miss the rod (diameter: 3 mm) of the target probe.

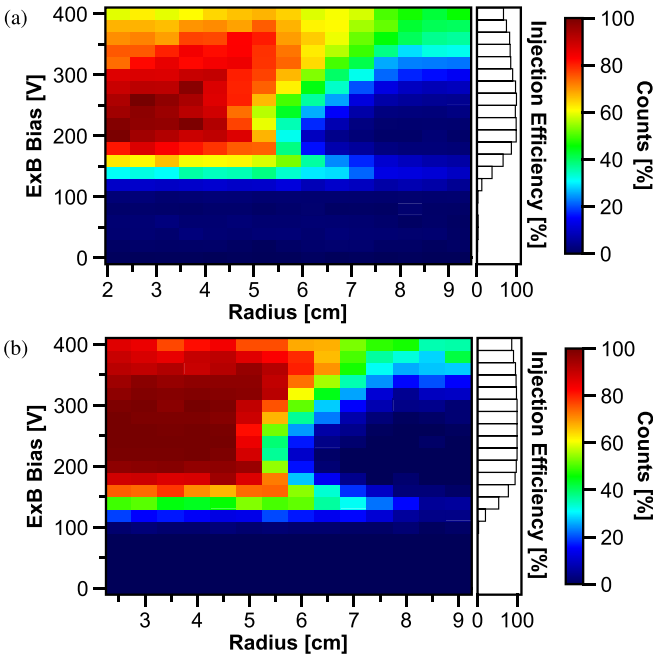


**FIG. 5.** 2D histogram of counts on the target probe as the radial positions of the probe and the E × B bias are varied. (a) Experiment with 5-eV positrons' injection. (b) Simulation using the same settings.

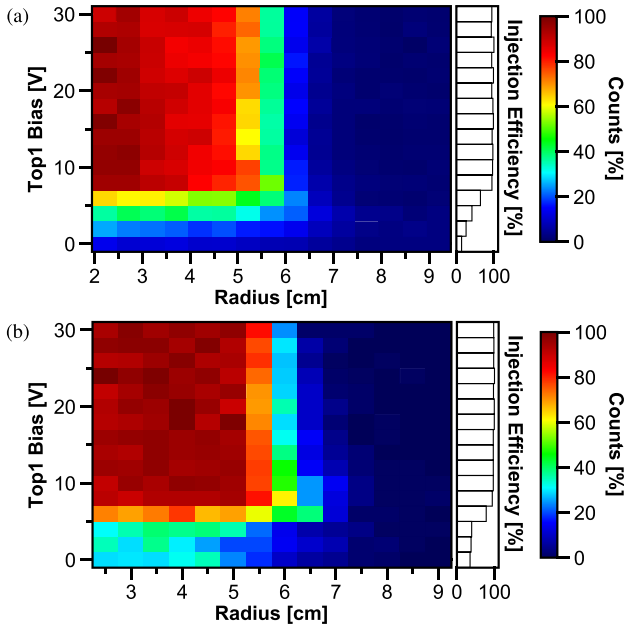


**FIG. 6.** Histogram of counts on the target probe as the probe is inserted and the Top1 bias is varied. (a) Experiment. (b) Simulation.

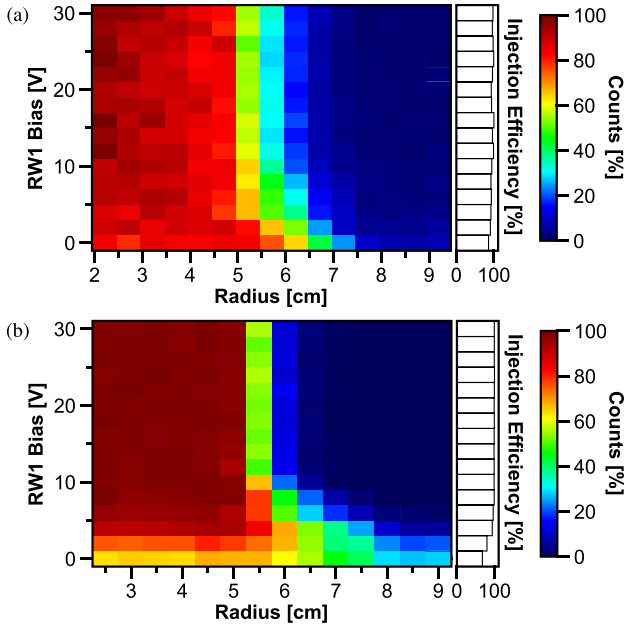


**FIG. 7.** Histogram of counts on the target probe as the probe is inserted and the RW1 bias is varied. (a) Experiment. (b) Simulation.

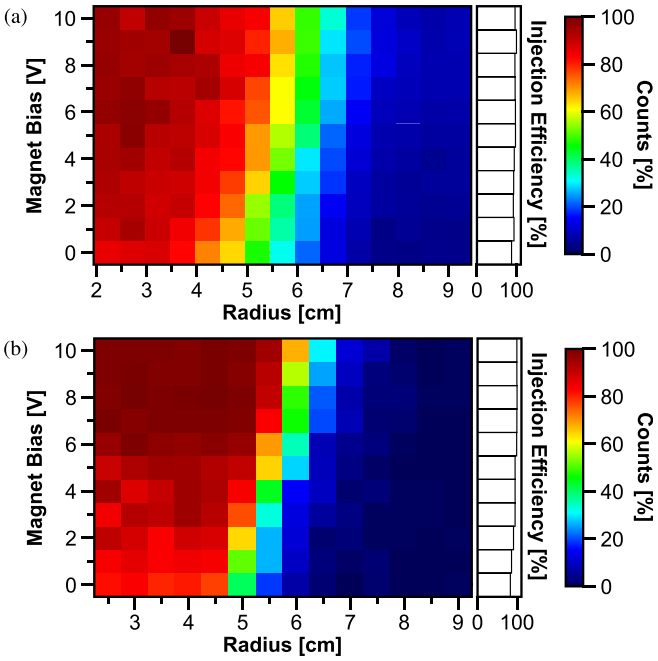


**FIG. 8.** Histogram of counts on the target probe as the probe is inserted and the magnet bias is varied. (a) Experiment. (b) Simulation.

So far, only one parameter was changed at a time. The multidimensional parameter space, however, is highly non-linear, which can be seen in Fig. 10. This simulation result shows how the $I_r - I_\theta$ region of good injection efficiency deforms with different E × B biases. It can

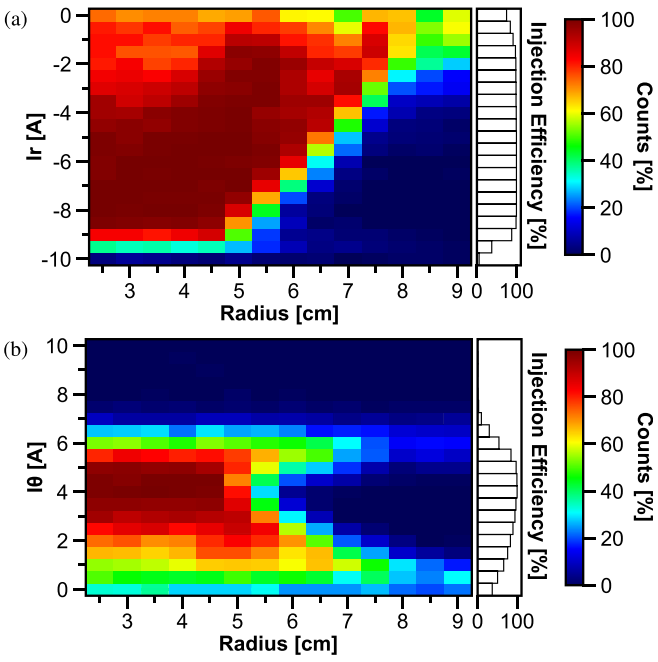


**FIG. 9.** Simulated histograms of counts on the target probe as it is inserted and the steering coil currents $I_r$ (a) and $I_\theta$ (b) are varied.

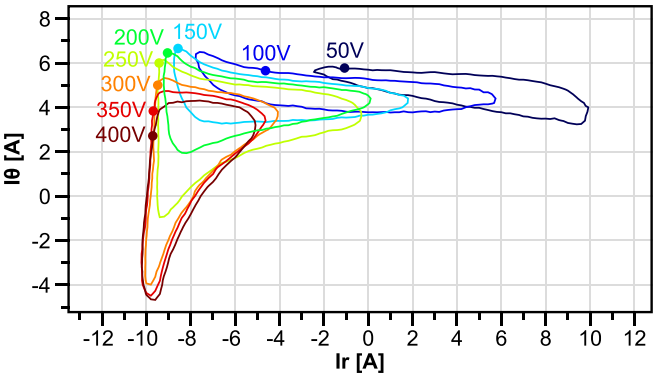


**FIG. 10.** $I_r - I_\theta$ steering coil current regions with >50% injection efficiency for different values of the E × B voltage.

be assumed that the radial distribution can be adjusted with even better control by changing multiple parameters at the same time.

These results confirm that the radial positron distribution can indeed be manipulated by varying the parameters of the experiment. Moreover, the simulation results agree very well with the experiment which is affirming for Secs. VI–VIII for which experimental data is not available.

## VI. TAILORING THE GUIDING CENTER DRIFT ORBITS

A valuable quantity for describing the motion of a charged particle in our magnetic dipole trap is the effective potential energy,[24] which is defined as

$$U_{eff} = e\phi_E + \mu B, \tag{3}$$

with the charge of the particle $e$, the electric potential $\phi_E$, the magnetic moment of the particle $\mu = mv_\perp^2/(2B)$, the mass of the particle $m$, the magnetic field strength $B$, and the perpendicular velocity $v_\perp$. Since the magnetic moment is an adiabatic invariant, the effective potential energy provides a means of visualizing where particles streaming along the magnetic field will be reflected in a way that combines electrostatic reflection with magnetic mirroring. The guiding center motion of a charged particle is therefore constrained by the effective potential boundary associated with its total energy.

Figure 11 shows vertical slices of simulated trajectories at three different azimuthal angles for particles with the same initial parallel kinetic energy, but with various values of their initial perpendicular kinetic energy. It also shows the contours where each particle's total energy equals the effective potential energy; reflection occurs at these surfaces. This figure shows the importance of the perpendicular energy spread of the incoming beam. In a trap with a stronger magnetic field, particles with a larger initial perpendicular velocity $v_{\perp 0}$ could be excluded from the confinement region entirely.

Since the electric potential of the E × B plates is anti-symmetric about the plane midway between the plates, the effective potential is asymmetric. This asymmetry forces particles continually toward the outer wall where they are finally lost after less than one toroidal rotation (Fig. 12). For this reason, confinement experiments involve switching off all electrodes except the magnet to establish a nearly symmetric trap in which charged particles can be confined for

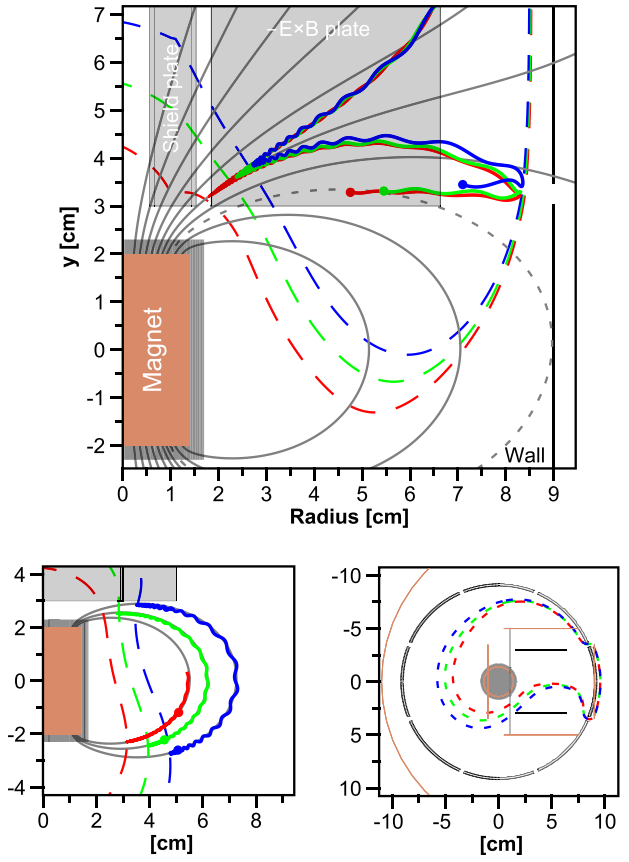


**FIG. 11.** Surfaces of maximum effective potential energy (dashed lines) for positrons with $E_0 = 5$ eV and different initial pitch angles $\alpha = \arctan(v_{\perp 0}/v_{\parallel 0})$. Red: $\alpha = 10°$, green: $\alpha = 20°$, and blue: $\alpha = 30°$. (a) shows the trajectories of these positrons during drift injection projected onto the vertical plane at a toroidal angle of 5°. The dot at the end of the trajectory indicates the particle position at this plane. The dotted field line (gray) defines the boundary of the confinement region. (b) shows the last parts of the trajectories of the same particles at a toroidal angle of 90° with the corresponding field lines and effective potential energy surfaces. (c) shows the extent of the effective potential energy surfaces at the mid-plane.

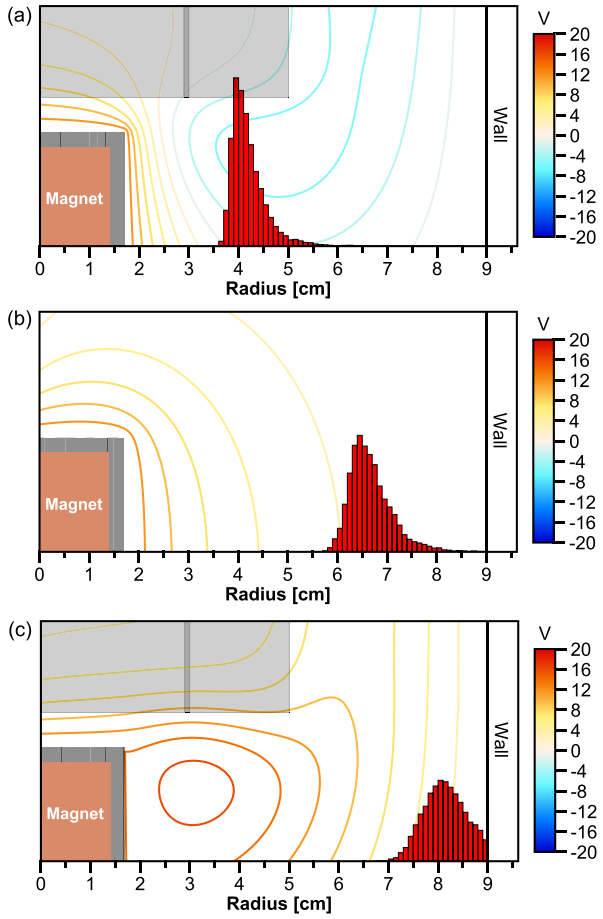


**FIG. 12.** Simulated radial distribution of 5000 positrons on the mid-plane at different toroidal angles (red histogram). (a) At 90° (b) at 180°, and (c) at 270°. The electric potential is illustrated by the contour lines.

thousands of toroidal rotations. The remaining asymmetries, which are caused by the off-axis beam line (Fig. 1) and the perturbation of the electric potential by the shield plate and E × B plates, are apparently not detrimental in Proto-APEX.

## VII. FROM INJECTION TO CONFINEMENT

In Sec. VI, we showed how the radial distribution evolves during a toroidal transit. This raises the question of what the distribution looks like for confined positrons—those that are trapped in the dipole field when the injection biases are switched off and which remain in the trap for tens or hundreds of thousands of toroidal transits.

The Proto-APEX experiment does not currently have the diagnostic capabilities to measure the radial and energy distribution of confined particles. However, this information is readily available from simulations. Figure 13 shows the total kinetic energy and radius of 10 000 injected and successfully trapped positrons. The integrated radial distribution (top bar chart, Fig. 13), looks similar to the distributions measured during injection experiments, with the exception that a population located close to the magnet appears with a high kinetic energy. This population (5%–10% of the total number trapped) consists of positrons that were close to the E × B region during the switch-off. Further simulations suggest that this population stays mostly confined even after the electrodes are switched on again to dump all confined positrons. For future pair plasma experiments, the presence of this high energy population is the cause for concern since energetic positrons annihilate more readily on residual gas molecules. In addition, to realize collective plasma effects, the average energy must be low to reach the short Debye length regime.

We are aware of the noticeable dependency of the energy on the final radial position, but the explanation is beyond the scope of this work.

In the experiment, only ∼360 positrons can be trapped at a time for each fill-hold-dump cycle due to the asymmetry of the electrostatic

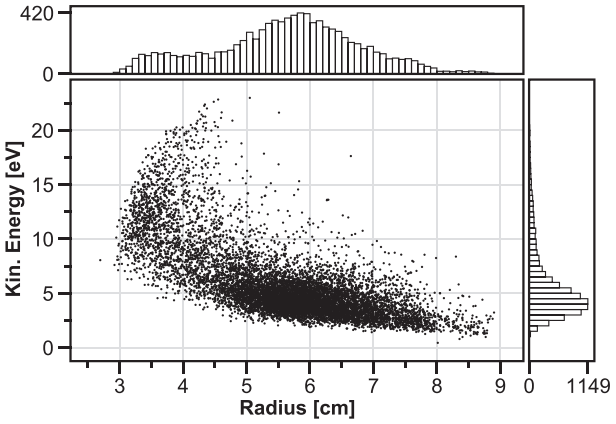


**FIG. 13.** Scatterplot of mid-plane crossing radius and total kinetic energy for 10 000 simulated positrons that were injected and confined. The potentials were switched off linearly within 1 $\mu$s. The histograms on the top and right show the sum of positrons with a given value.

field, as discussed in Sec. VI. To achieve plasma densities, it will be necessary to first store and accumulate positrons from the continuous NEPOMUC beam, and then inject all the positrons in one short pulse.[5] Such an accumulation system is currently being developed alongside APEX.

## VIII. DIFFUSION IN POSITION AND VELOCITY SPACE

In an ideal world, the radial and energy distribution of the trapped positron population would not evolve further, since it is firmly in the single-particle regime due to the extremely low densities. In reality, residual gas molecules are present due to the imperfect vacuum ($\sim 5 \times 10^{-8}$ mbar). Elastic collision with these neutrals is the dominant collision process; this results in velocity-space and position-space diffusion and currently limits confinement time in Proto-APEX. Particles with more energy than the bias of the magnet can scatter into its loss cone and annihilate on it; meanwhile, slower radial diffusion allows particles to move across field lines. Simulations have found the characteristic number of collisions for positrons to reach an electrode on which they can annihilate (primarily, the shield and E × B plates) to agree well with the experimentally measured confinement times, as reported previously.[14] Simulations also provide a picture of the evolution of positrons' radial distribution.

In the simulation, elastic scattering was implemented as a simple randomization of the direction of the velocity vector. Since the collision frequency in the experiment is too low to be simulated in a reasonable amount of computing time, the collision frequency in the simulation was set to be 1 MHz as opposed to ~150 Hz expected from the mean free path at the given vacuum pressure. This is of the order of the bounce motion back and forth between the magnet's poles (1–10 MHz), much slower than the cyclotron frequency (0.1–10 GHz), but faster than the frequency of the toroidal drift (10–100 kHz). Figure 14 shows the position diffusion after ten scattering events of particles that were initially launched from the mid-plane with a delta function distribution at different radii, and with $E_{\|0} = 5$ eV and $E_{\perp 0} = 1$ eV. One can see that the radial diffusion is faster at larger radii because each collision changes the position by an amount on the

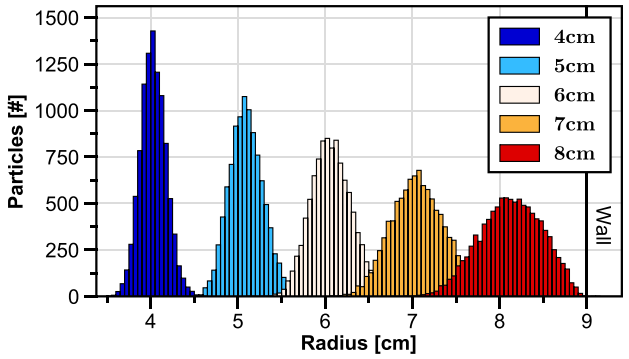


**FIG. 14.** Positrons with $E_{\|0} = 5$ eV and $E_{\perp 0} = 1$ eV were started at different radii. The histograms show the radial distribution after ten collisions. All electrodes are grounded.

order of the Larmor radius, which is larger further away from the magnet where the magnetic field is weaker.

When positrons diffuse outwards far enough, they can collide with the E × B plates and shield plate, since they extend into the confinement region [as illustrated in Fig. 11(a)]. This has been identified as a major loss mechanism.[14] More recent simulations have shown that the shield plate and the E × B plates can be shortened by 2.5 cm (Fig. 15) without having to change any other parameters and without deteriorating the injection efficiency. If the parameters are adjusted appropriately, the plates can be as short as 1 cm since the fringe field is

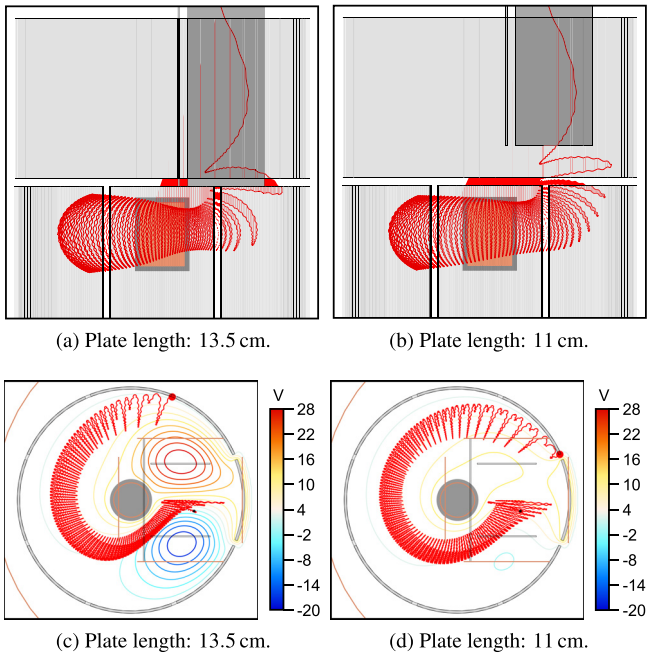


(a) Plate length: 13.5 cm. (b) Plate length: 11 cm.

(c) Plate length: 13.5 cm. (d) Plate length: 11 cm.

**FIG. 15.** Comparison of trajectory simulations done with the experimental setup (a) and (c) used so far and the shorter shield plate and E × B plates (b) and (d). The contours correspond to the electric potential in the mid-plane. A sample positron trajectory with $E_{\|0} = 5$ eV and $E_{\perp 0} = 0.5$ eV is shown in red.

still able to E × B drift inject particles into the trap without significant loss. These shorter plates, which do not extend into the confinement region, should allow for longer confinement times, since positrons cannot intersect them anymore and are able to drift outwards until they hit the outer wall. Another benefit of shorter E × B plates is that positrons are perturbed less by their electric fields which leads to more positrons being trapped in each fill-hold-dump cycle and therefore increasing the signal-to-noise ratio.

## IX. CONCLUSION

APEX has the goal to create an electron–positron plasma in a magnetic dipole trap. In the test setup with a permanent magnet, a grounded target probe is used to measure the radial distribution of positrons in the trap by inserting it stepwise into the confinement region. It was shown by simulations that the target probe provides a good measurement, despite perturbing the positron trajectories when fully inserted.

Because the radial deposition of positrons plays an important role in different experiments, we investigated how the free parameters (electrode biases and steering coil currents) affect where the trap positrons are injected. Both experimental data and simulations showed that the bias of the magnetic case and the steering coil current $I_r$ can be used to manipulate the radial deposition. Many of the parameters we have studied have a broad acceptance range, and some are quite nonlinear, so the adjustment of multiple parameters at once could provide even more control over the radial deposition.

Furthermore, we explained that describing the electromagnetic fields in terms of the effective potential is a helpful tool to understand the behavior of positrons during injection.

A crucial element to study an electron–positron plasma is the duration of confinement. The simulations discovered an important heating mechanism that occurs at the end of the injection phase when the E × B plates are switched off, leading to a positron population with high energy close to the magnet. We also looked at how the radial distribution is altered by elastic scattering and that outward diffusion with subsequent collision with the E × B plates and shield plate is a major loss process which can be easily avoided by shortening these plates.

The understanding of these effects and the good agreement between the simulation and experiment is of great value for interpreting the experimental results, designing future experiments, and pushing the development of a pair plasma device forward.

## ACKNOWLEDGMENTS

This work is based upon experiments performed at the NEPOMUC positron beam facility operated by FRM II at the Heinz Maier-Leibnitz Zentrum (MLZ), Garching, Germany. The work received funding from the European Research Council (ERC) under the European Union's Horizon 2020 research and innovation programme under Grant Agreement No. 741322. Furthermore, the authors thank the DFG (Nos. Hu 978/15-1 and Sa 2788/2-1), JSPS KAKENHI (Nos. 25707043 and 16KK0094), U. S. DOE grant DE-SC0019271, the UCSD Foundation and the Helmholtz Postdoc Programme (E.V.S.) for the funding.

## APPENDIX: PARAMETER SETTINGS

**TABLE I.** Parameter settings of the experiments and simulations.

| Figures | $I_r$ (A) | $I_\theta$ (A) | E × B (V) | Magnet (V) | Top1 (V) | Top2 (V) | RW1 (V) | RW2-8 (V) |
|---|---|---|---|---|---|---|---|---|
| 2(a) | −8.3 | 4 | 220 | 0 | 14 | 0 | 20 | 0 |
| 2(b) | −8.3 | 4 | 220 | 30 | 14 | 0 | 20 | 0 |
| 4 | −8.3 | 4 | 220 | 8 | 14 | 0 | 14 | 0 |
| 5 | −8.3 | 4 | … | 8 | 14 | 0 | 20 | 0 |
| 6 | −8 | 4 | 180 | 8 | … | 0 | 14 | 0 |
| 7 | −8 | 4 | 200 | 8 | 22 | 0 | … | 0 |
| 8 | −8.3 | 4 | 220 | … | 14 | 14 | 20 | 0 |
| 9(a) | … | 4 | 220 | 8 | 14 | 0 | 20 | 0 |
| 9(b) | −8.3 | … | 220 | 8 | 14 | 0 | 20 | 0 |
| 10 | … | … | … | 0 | 12 | 0 | 12 | 0 |
| 11 | −9 | 4 | 210 | 12 | 12 | 0 | 12 | 0 |
| 12 | −9 | 3 | 210 | 12 | 12 | 0 | 12 | 0 |
| 13 | −8.3 | 4 | 220 | 8 | 14 | 0 | 22 | 0 |
| 14 | 0 | 0 | 0 | 0 | 0 | 0 | 0 | 0 |
| 15 | −9 | 3 | 210 | 12 | 12 | 0 | 12 | 0 |

## DATA AVAILABILITY

The data that support the findings of this study are available from the corresponding author upon reasonable request.

## REFERENCES

[1]G. P. Zank and R. G. Greaves, "Linear and nonlinear modes in nonrelativistic electron-positron plasmas," Phys. Rev. E **51**, 6079 (1995).
[2]P. Helander, "Microstability of magnetically confined electron-positron plasmas," Phys. Rev. Lett. **113**, 135003 (2014).
[3]G. Sarri, M. E. Dieckmann, I. Kourakis, A. D. Piazza, B. Reville, C. H. Keitel, and M. Zepf, "Overview of laser-driven generation of electron-positron beams," J. Plasma Phys. **81**, 455810401 (2015).
[4]H. Higaki, C. Kaga, K. Fukushima, H. Okamoto, Y. Nagata, Y. Kanai, and Y. Yamazaki, "Simultaneous confinement of low-energy electrons and positrons in a compact magnetic mirror trap," New J. Phys. **19**, 023016 (2017).
[5]T. S. Pedersen, J. R. Danielson, C. Hugenschmidt, G. Marx, X. Sarasola, F. Schauer, L. Schweikhard, C. M. Surko, and E. Winkler, "Plans for the creation and studies of electron-positron plasmas in a stellarator," New J. Phys. **14**, 035010 (2012).
[6]M. R. Stoneking, H. Saitoh, M. Singer, E. V. Stenson, J. Horn-Stanja, T. S. Pedersen, S. Nißl, U. Hergenhahn, N. Yanagi, C. Hugenschmidt, M. Dickmann, J. R. Danielson, and C. M. Surko, "Toward a compact levitated superconducting dipole for positron-electron plasma confinement," AIP Conf. Proc. **1928**, 020015 (2018).
[7]A. Hasegawa, "A dipole field fusion reactor," Comments Plasma Phys. Controlled Fusion **11**, 147–151 (1987).
[8]A. C. Boxer, R. Bergmann, J. L. Ellsworth, D. T. Garnier, J. Kesner, M. E. Mauel, and P. Woskov, "Turbulent inward pinch of plasma confined by a levitated dipole magnet," Nat. Phys. **6**, 207–212 (2010).
[9]Z. Yoshida, Y. Ogawa, J. Morikawa, S. Watanabe, Y. Yano, S. Mizumaki, T. Tosaka, Y. Ohtani, A. Hayakawa, and M. Shibui, "First plasma in the RT-1 device," Plasma Fusion Res. **1**, 008 (2006).
[10]H. Saitoh, T. S. Pedersen, U. Hergenhahn, E. V. Stenson, N. Paschkowski, and C. Hugenschmidt, "Recent status of a positron-electron experiment (APEX)," J. Phys. **505**, 012045 (2014).
[11]E. V. Stenson, H. Saitoh, J. Stanja, H. Niemann, U. Hergenhahn, T. S. Pedersen, G. H. Marx, L. Schweikhard, J. R. Danielson, C. M. Surko *et al.*, "Progress

toward positron-electron pair plasma experiments," AIP Conf. Proc. **1668**, 040004 (2015).
[12]E. V. Stenson, "Plans for EPOS: A tabletopsized, superconducting, optimized stellarator for matter/antimatter pair plasmas," Stellarator News **2019**, 167.
[13]E. V. Stenson, S. Nißl, U. Hergenhahn, J. Horn-Stanja, M. Singer, H. Saitoh, T. S. Pedersen, J. R. Danielson, M. R. Stoneking, and M. Dickmann, "Lossless positron injection into a magnetic dipole trap," Phys. Rev. Lett. **121**, 235005 (2018).
[14]J. Horn-Stanja, S. Nißl, U. Hergenhahn, T. S. Pedersen, H. Saitoh, E. V. Stenson, M. Dickmann, C. Hugenschmidt, M. Singer, and M. R. Stoneking, "Confinement of positrons exceeding 1 s in a supported magnetic dipole trap," Phys. Rev. Lett. **121**, 235003 (2018).
[15]C. Hugenschmidt, H. Ceeh, T. Gigl, F. Lippert, C. Piochacz, P. Pikart, M. Reiner, J. Weber, and S. Zimnik, "The upgrade of the neutron induced positron source NEPOMUC," J. Phys. **443**, 012079 (2013).
[16]J. Horn-Stanja, E. V. Stenson, M. R. Stoneking, M. Singer, U. Hergenhahn, S. Nißl, H. Saitoh, T. S. Pedersen, M. Dickmann, and C. Hugenschmidt, "Injection of intense low-energy reactor-based positron beams into a supported magnetic dipole trap," Plasma Res. Express **2**, 015006 (2020).
[17]J. Stanja, U. Hergenhahn, H. Niemann, N. Paschkowski, T. S. Pedersen, H. Saitoh, E. V. Stenson, M. R. Stoneking, C. Hugenschmidt, and C. Piochacz, "Characterization of the NEPOMUC primary and remoderated positron beams at different energies," Nucl. Instrum. Methods Phys. Res., Sect. A **827**, 52–62 (2016).
[18]J. C. Simpson, J. E. Lane, C. D. Immer, and R. C. Youngquist, "Simple analytic expressions for the magnetic field of a circular current loop," NASA Technical Report No. 20010038494 (2001).
[19]M. Misakian, "Equations for the magnetic field produced by one or more rectangular loops of wire in the same plane," J. Res. Natl. Inst. Stand. Technol. **105**, 557 (2000).
[20]T. L. Tang, see https://nukephysik101.files.wordpress.com/2011/07/finite-length-solenoid-potential-and-field.pdf for "Finite Length Solenoid Potential and Field, 2011."
[21]NIST Digital Library of Mathematical Functions, Section 19.8, edited by F. W. J. Olver, A. B. Olde Daalhuis, D. W. Lozier, B. I. Schneider, R. F. Boisvert, C. W. Clark, B. R. Miller and B. V. Saunders (NIST, 2018).
[22]P. O. J. Scherer, *Computational Physics* (Springer, 2010), Chap. 17, p. 308.
[23]P. M. Bellan, *Fundamentals of Plasma Physics* (Cambridge University Press, 2008).
[24]A. H. Boozer, "Time-dependent drift Hamiltonian," Phys. Fluids **27**, 2441–2445 (1984).